Available online at www.sciencedirect.com
SCIENCE DIRECT®
Journal of Sound and Vibration 280 (2005) 1051–1065
JOURNAL OF SOUND AND VIBRATION
www.elsevier.com/locate/jsvi

Short Communication

Dynamic stability of a submerged, free-hanging riser conveying fluid

G.L. Kuiper*, A.V. Metrikine

Faculty of Civil Engineering and Geosciences, Delft University of Technology, P.O. Box 5048, 2600 GA Delft, Netherlands

Received 10 November 2003; accepted 29 September 2004

Abstract

Studying the stability of a vertically suspended, fully submerged pipe conveying water (water riser), researchers have found a contradiction between theoretical predictions and experiments. Theory predicts instability at small velocities of convection, while experiments did not show such instability. The only attempt to explain this contradiction was made by Païdoussis, suggesting that the theoretical prediction is wrong because of an improper description of the negative pressurisation of water at the inlet of the pipe. In this paper, it is shown theoretically that the negative pressurisation influences the stability only slightly and cannot explain the contradiction. What can explain it, is the hydrodynamic drag caused by surrounding water, which is shown to be an essential stabilising factor.

1. Introduction

Cantilevered (fixed-free) pipes conveying fluid behave non-conservatively [1,2], implying that the energy of the pipe–fluid system varies in time. The energy increases or decreases depending on the direction of the fluid flow. If the fluid is sucked into the pipe at the free end and no damping is regarded, the energy of the pipe grows ever since it starts moving, so that the pipe is *unstable*.

*Corresponding author. Tel.: +31 15 2784671; fax: +31 15 2785767.
E-mail addresses: G.L.Kuiper@citg.tudelft.nl (G.L. Kuiper), A.Metrikine@citg.tudelft.nl (A.V. Metrikine).

0022-460X/$ - see front matter © 2004 Elsevier Ltd. All rights reserved.
doi:10.1016/j.jsv.2004.09.024

A pipe hanging in water loses its energy while moving due to the hydrodynamic drag, which may alter the pipe stability.

Cantilever pipes can be used in ocean mining to transport a mixture of water and nodules from the sea bottom to a ship [3]. Recently, designs have been made for pipes suspended from a floating barge, which will be used for pumping up cooling water. These pipes have an unconstrained tip (lower end) and therefore are referred to as *free-hanging risers*. A question arises whether these risers might become unstable while conveying fluid?

According to existing theory, a free-hanging riser can be unstable at very low convection speed of the flow in the pipe. However, there is a contradiction between theory and experiments. The theory predicts unstable behaviour for undamped pipes at infinitely small fluid velocity [4–6]. On the contrary, in experiments with submerged, cantilevered pipes pumping up water (see Ref. [7]), no instability has been observed. Later, Païdoussis [8] explained in a short way why these cantilevered pipes should behave stable. The main reason, according to this explanation, is negative pressurisation of the fluid at the inlet of the riser.

In this paper, it is shown that this negative pressurisation has a slight influence on the system stability and, therefore, cannot be considered as an explanation for experimentally observed stable behaviour of free-hanging pipes. As shown in this paper, the experimental results can be explained by the stabilising effect of the hydrodynamic drag caused by the surrounding water.

This paper is structured as follows. In Section 2, the equation of motion is presented of a submerged, free-hanging riser conveying fluid, and the main assumptions are discussed with which this equation is applicable. In literature, different models are available for description of the fluid pressure inside the riser, which are treated in Section 3. Section 4 shows the non-dimensional equation of motion and the boundary conditions for the riser. In Section 5, the characteristic equation for small bending motion of the riser is obtained. The roots of this equation are analysed in Section 6 by using the Argand diagram. To study the effect of the fluid pressurisation at the inlet and of the hydrodynamic drag on the system stability, the D-decomposition method [9,10] is employed. This method is complementary to the conventional Argand diagram and is proved to be instrumental for stability analyses (see Refs. [11,12]). The method is briefly outlined in Section 7 and applied in Section 8.

2. Assumptions and equation of motion

Consider a straight riser that conveys water up to a floating barge as shown in Fig. 1. The riser is tubular and submerged fully. It is attached to the barge through a so-called flex-joint connection that fixes the translational motion of the riser top to that of the barge and provides a linear-elastic reaction against a relative angular motion of the barge and the riser top. The tip of the riser is free (not constrained); accordingly, the riser is referred to as a *free-hanging riser*. Dynamics of the riser is studied in this paper under the following assumptions:

(a) The riser moves in the plane that is depicted in Fig. 1.
(b) The length of the riser and the wavelength of its deformation are large in comparison to the diameter of the riser, so that the Euler–Bernoulli theory is applicable for the bending of the riser and the plug-flow model [7] is acceptable.

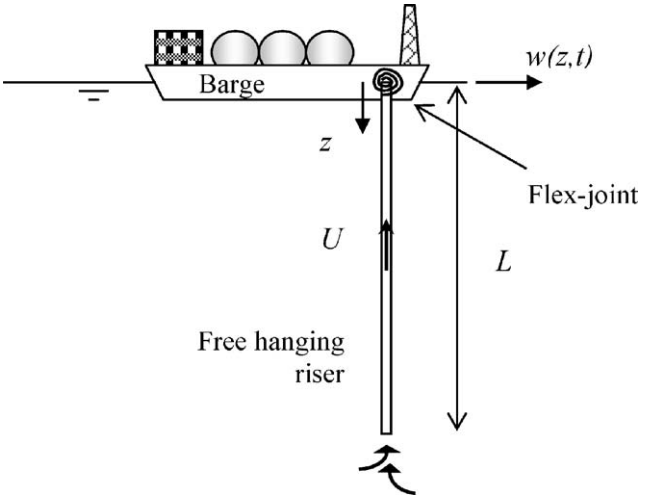

Fig. 1. Sketch of a free-hanging riser conveying fluid.

(c) Small bending motion of the riser about its equilibrium position is considered.
(d) The pipe wall behaves elastically, i.e. no internal damping is considered.
(e) The vertical motion of the barge is disregarded.
(f) The flow inside the riser is uniform across the riser and its mean velocity along the riser is constant.
(g) No friction between the fluid flow and the riser is accounted for.

With these assumptions, the equation that governs the horizontal motion of a differential element of the riser can be written as

$$EI\frac{\partial^4 w}{\partial z^4} - \frac{\partial}{\partial z}\left(T_r(z)\frac{\partial w}{\partial z}\right) + \rho_f A_i\left(U^2\frac{\partial^2 w}{\partial z^2} - 2U\frac{\partial^2 w}{\partial z \partial t} + \frac{\partial^2 w}{\partial t^2}\right) - \frac{\partial}{\partial z}\left((A_e p_e(z) - A_i p_i(z))\frac{\partial w}{\partial z}\right) + \rho_r A_r\frac{\partial^2 w}{\partial t^2} = f(z,t), \quad (1)$$

where $w(z,t)$ is the horizontal riser displacement, z the coordinate along the riser (directed downward), t the time, EI the bending stiffness of the riser, $T_r(z)$ the axial tension of the riser, ρ_r and ρ_f the mass density of the riser and the fluid, respectively, A_i and A_e the internal and external cross-sectional areas of the riser, respectively, $A_r = A_e - A_i$ the cross-sectional area of the pipe wall, $p_i(z)$ and $p_e(z)$ the water pressure inside and outside the riser, respectively, U the velocity of the flow through the riser (directed upward), and $f(z,t)$ the normal dynamic reaction of the surrounding water on the riser element.

The first and last terms on the left-hand side of Eq. (1) form the well-known equation for the bending motion of a beam according to the Euler–Bernoulli theory. The second term, $\partial/\partial_z(T_r(z)\partial w/\partial z)$, is due to the longitudinal tension in the riser that is caused by gravity, minus the hydrostatic pressure on the rim of the riser tip. This tension reads

$$T_r(z) = \rho_r A_r g(L - z) - \rho_f A_r g L, \quad (2)$$

where g is the gravity acceleration and L the length of the riser (see Fig. 1). Note that the origin of the reference system is fixed to the riser top. The third term on the left-hand side of Eq. (1) is the transverse loading per unit length exerted by the internal flow on the pipe. This term is well known in dynamics of pipes conveying fluid and is explained in detail in the book of Païdoussis [7]. The fourth term in Eq. (1), $\partial/\partial_z((A_e p_e(z) - A_i p_i(z))\partial w/\partial_z)$, is due to the pressure on the pipe wall. The external hydrostatic pressure $p_e(z)$, neglecting the temperature effects (and compressibility, as mentioned above), may be assumed to vary linearly with z, so that

$$p_e(z) = \rho_f g z. \tag{3}$$

The description of the internal pressure, which is the key issue of this development, is discussed in detail in the next section.

The dynamic reaction of the surrounding water on the riser, $f(z,t)$, is assumed to be a superposition of an inertia force $f_{\text{in}}(z,t)$ and a drag force $f_d(z,t)$. The inertia force depends on the acceleration of the riser and of the surrounding water as

$$f_{\text{in}}(z,t) = \rho_f A_e (C_a + 1)\frac{\partial u}{\partial t} - \rho_f A_e C_a \frac{\partial^2 w}{\partial t^2}, \tag{4}$$

where $u(z,t)$ is the horizontal component of the surrounding water velocity and C_a the added mass coefficient. The drag force depends on the relative motion of the riser and on the surrounding water nonlinearly. Besides, the drag force is influenced by Reynolds number, wall surface roughness, water turbulence, etc. In this study, all these effects and the nonlinearity are neglected. The only aim of incorporating the external damping is to investigate whether this might explain the difference between theory and experiments. Hence, the following linearised expression for the drag force is used (see Ref. [7]):

$$f_d(z,t) = \tfrac{1}{2}\rho_f D_0 \tilde{C}_d \left(u - \frac{\partial w}{\partial t}\right), \tag{5}$$

where $\tilde{C}_d$ is the adapted drag coefficient, with the dimension of velocity.

3. Description of the internal pressure

The internal water pressure $p_i(z)$ in pipes sucking up fluid is a subject of discussion in literature. There exist two different opinions about the description of the internal pressure. Païdoussis and Luu [4] assumed that the internal pressure does not differ from the external one (at the same depth) and, accordingly, it does not depend on the speed of the internal fluid flow. This approach was also used by Sällström and Åkesson [5] and by Kangaspuoskari et al. [6]. All these papers reported unstable behaviour of the free-hanging, undamped riser sucking up fluid at infinitely small flow velocity.

Recently, Païdoussis [8] suggested that there is a negative pressurisation at the riser tip so that the difference between the external and internal pressure is equal to $\rho_f U^2$. This pressure difference is in agreement with the pressure drop in a so-called Borda's mouthpiece, which is a short tube of length almost equal to the radius that projects into a reservoir. At the inlet the coefficient of contraction for the Borda's mouthpiece is 0.5. By modelling the internal pressure

in this way, the pressure drop balances the centrifugal force induced by the internal flow ($\rho_f A_i U^2 \partial^2 w/\partial z^2$). In this case, the only remaining term in the equation of motion, Eq. (1), related to the fluid velocity is the Coriolis force. Païdoussis concluded that no flutter, and hence no instability, can occur if only the Coriolis force is present. In this paper, it is shown that this conclusion is incorrect.

Modification of the geometry of the inlet can reduce the pressure loss. If the inlet is shaped so that the fluid flow remains fully attached to the wall, no pressure loss occurs at the inlet. In this theoretical case without contraction, the Bernoulli equation shows that the difference between the external and internal pressure is equal to $\rho_f U^2/2$. In reality, the pressure difference depends on the geometry of the inlet and varies between $\rho_f U^2/2$ and $\rho_f U^2$.

The effect of the magnitude of the pressure difference has never been studied in the literature, to the authors' knowledge. Therefore, in what follows, vibrations are studied of the riser for all the three aforementioned internal pressure drops and results are compared to each other. Thus, the following expressions for the internal pressure are considered:

$$p_i(z) = \rho_f g z - \Delta p^{(k)}, \quad k = 1,2,3 \quad \text{with } \Delta p^{(1)} = 0,\ \Delta p^{(2)} = \rho_f U^2,\ \Delta p^{(3)} = \tfrac{1}{2}\rho_f U^2. \tag{6}$$

4. Dimensionless form of the equation of motion and the boundary conditions

Substituting Eqs. (2)–(6) into the equation of motion, Eq. (1), the latter can be rewritten in the following form:

$$\begin{aligned} EI\frac{\partial^4 w}{\partial z^4} + \left(m_f U^2 - \Delta p^{(k)} A_i + T_{\text{top}}\left(\frac{z}{L} - 1\right)\right)\frac{\partial^2 w}{\partial z^2} + \frac{T_{\text{top}}}{L}\frac{\partial w}{\partial z} - 2m_f U\frac{\partial^2 w}{\partial z \partial t} \\ + \tfrac{1}{2}\rho_f D_0 \tilde{C}_d \frac{\partial w}{\partial t} + (m_r + m_a + m_f)\frac{\partial^2 w}{\partial t^2} = m_f (C_a + 1)\frac{\partial u}{\partial t} + \tfrac{1}{2}\rho_f D_0 \tilde{C}_d u, \end{aligned} \tag{7}$$

where $m_r = \rho_r A_r$, $m_a = \rho_f C_a A_e$, $m_f = \rho_f A_i$, $T_{\text{top}} = (\rho_r - \rho_f) A_r g L$.

The external forces (external flow) do not affect the stability of the system within the accepted linearised model. Consequently, the right-hand side of the equation of motion is disregarded from hereonwards.

The boundary conditions at the ends of the pipe are given as

$$w(0,t) = 0, \quad EI\frac{\partial^2 w(0,t)}{\partial z^2} = C_{fl}\frac{\partial w(0,t)}{\partial z}, \quad EI\frac{\partial^2 w(L,t)}{\partial z^2} = 0, \quad EI\frac{\partial^3 w(L,t)}{\partial z^3} = 0, \tag{8}$$

where C_{fl} is the stiffness of the rotational spring at the top of the riser. Introducing the following dimensionless variables and parameters:

$$\begin{aligned} &\eta = w/L, \quad \xi = z/L, \quad \tau = t\sqrt{EI/(m_r + m_a + m_f)}/L^2, \quad V = U\sqrt{m_f/T_{\text{top}}}, \\ &\alpha = T_{\text{top}} L^2/EI, \quad \beta = L\sqrt{m_f T_{\text{top}}}/\sqrt{EI(m_r + m_a + m_f)}, \\ &\gamma = \rho_f D_0 \tilde{C}_d L^2/\left(2\sqrt{EI(m_r + m_a + m_f)}\right), \quad C^{(k)} = \Delta p^{(k)} A_i/T_{\text{top}}, \quad \kappa = C_{fl} L/EI, \end{aligned}$$

the statement of the problem Eqs. (7) and (8) is rewritten as

$$\frac{\partial^4\eta}{\partial\xi^4}+\alpha(V^2-C^{(k)}-1)\frac{\partial^2\eta}{\partial\xi^2}+\alpha\xi\frac{\partial^2\eta}{\partial\xi^2}+\alpha\frac{\partial\eta}{\partial\xi}-2\beta V\frac{\partial^2\eta}{\partial\xi\partial\tau}+\gamma\frac{\partial\eta}{\partial\tau}+\frac{\partial^2\eta}{\partial\tau^2}=0, \tag{9}$$

$$\eta(0,\tau)=0,\quad \frac{\partial^2\eta(0,\tau)}{\partial\xi^2}=\kappa\frac{\partial\eta(0,\tau)}{\partial\xi},\quad \frac{\partial^2\eta(1,\tau)}{\partial\xi^2}=0,\quad \frac{\partial^3\eta(1,\tau)}{\partial\xi^3}=0. \tag{10}$$

In Eq. (9), the coefficient $C^{(k)}$ changes for the three descriptions of the pressure difference:

$$\Delta p^{(1)}=0 \quad \text{corresponds to } C^{(1)}=0,$$
$$\Delta p^{(2)}=\rho_f U^2 \quad \text{corresponds to } C^{(2)}=V^2,$$
$$\Delta p^{(3)}=\tfrac{1}{2}\rho_f U^2 \quad \text{corresponds to } C^{(3)}=\tfrac{1}{2}V^2.$$

5. Characteristic equation

To find the eigenvalues of the problem Eqs. (9) and (10), the displacement $\eta(\xi,\tau)$ is to be sought in the following form:

$$\eta(\xi,\tau)=W(\xi)\mathrm{e}^{\lambda\tau}. \tag{11}$$

The pipe is unstable if at least one of the eigenvalues λ has a positive real part.

Substituting Eq. (11) into the equation of motion, Eq. (10), the following ordinary differential equation is obtained:

$$\frac{\mathrm{d}^4W}{\mathrm{d}\xi^4}+\alpha(V^2-C^{(k)}-1)\frac{\mathrm{d}^2W}{\mathrm{d}\xi^2}+\alpha\xi\frac{\mathrm{d}^2W}{\mathrm{d}\xi^2}+\alpha\frac{\mathrm{d}W}{\mathrm{d}\xi}-2\beta V\lambda\frac{\mathrm{d}W}{\mathrm{d}\xi}+\gamma\lambda W+\lambda^2W=0. \tag{12}$$

This dimensionless ordinary differential equation contains one coefficient that depends on ξ, which implies that the eigenfunctions of this equation are not sinusoidal. A solution to this equation can be sought in the form of a power series expansion (see Ref. [13]):

$$W(\xi)=\sum_{n=0}^{\infty}a_n\xi^n. \tag{13}$$

Substituting Eq. (13) into Eq. (12), an equation is obtained involving a power series whose sum is equal to zero. Since each term in the series must be equal to zero, the following recurrence relation can be derived:

$$a_n=A_{n-2}a_{n-2}+A_{n-3}a_{n-3}+A_{n-4}a_{n-4}\quad (n\geqslant 4), \tag{14}$$

with

$$A_{n-2}=\frac{-\alpha(V^2-C^{(k)}-1)}{n(n-1)},\quad A_{n-3}=\frac{-(\alpha(n-3)-2\beta V\lambda)}{n(n-1)(n-2)},\quad A_{n-4}=\frac{-(\gamma\lambda+\lambda^2)}{n(n-1)(n-2)(n-3)}.$$

By repeated application of this recurrence relation, starting with $n = 4$, a_n can be expressed as a linear combination of a_0, a_1, a_2 and a_3:

$$a_n = F_n a_0 + G_n a_1 + H_n a_2 + I_n a_3 \quad (n \geqslant 0), \tag{15}$$

in which

$$\begin{aligned} &F_0 = 1, \quad F_1 = 0, \quad F_2 = 0, \quad F_3 = 0, \\ &G_0 = 0, \quad G_1 = 1, \quad G_2 = 0, \quad G_3 = 0, \\ &H_0 = 0, \quad H_1 = 0, \quad H_2 = 1, \quad H_3 = 0, \\ &I_0 = 0, \quad I_1 = 0, \quad I_2 = 0, \quad I_3 = 1. \end{aligned} \tag{16}$$

By substituting Eq. (15) into Eq. (14) the following relations are found:

$$\begin{bmatrix} F_n \\ G_n \\ H_n \\ I_n \end{bmatrix} = A_{n-2} \begin{bmatrix} F_{n-2} \\ G_{n-2} \\ H_{n-2} \\ I_{n-2} \end{bmatrix} + A_{n-3} \begin{bmatrix} F_{n-3} \\ G_{n-3} \\ H_{n-3} \\ I_{n-3} \end{bmatrix} + A_{n-4} \begin{bmatrix} F_{n-4} \\ G_{n-4} \\ H_{n-4} \\ I_{n-4} \end{bmatrix}. \tag{17}$$

With the starting values given by Eq. (16), it is possible to obtain F_n, G_n, H_n and I_n for every n. Making use of Eq. (15), the general solution Eq. (13) can then be written as

$$W(\xi) = a_0 \sum_{n=0}^{\infty} F_n \xi^n + a_1 \sum_{n=0}^{\infty} G_n \xi^n + a_2 \sum_{n=0}^{\infty} H_n \xi^n + a_3 \sum_{n=0}^{\infty} I_n \xi^n. \tag{18}$$

To find the four unknowns a_j, $j = 0, \ldots, 3$, Eq. (18) should be substituted into the boundary conditions, Eq. (10). This yields four linear algebraic equations with respect to a_0–a_3. From the first two boundary conditions of Eq. (10), it is concluded that

$$a_0 = 0 \quad \text{and} \quad a_2 = \frac{\kappa}{2} a_1. \tag{19}$$

Using Eqs. (18) and (19), the last two boundary conditions of Eq. (10) result in the following equations:

$$\begin{aligned} a_1(a + \kappa b) + a_3 c = 0, \\ a_1(d + \kappa e) + a_3 f = 0, \end{aligned} \tag{20}$$

with

$$a = \sum_{n=2}^{\infty} G_n n(n-1), \quad b = \frac{1}{2} \sum_{n=2}^{\infty} H_n n(n-1), \quad c = \sum_{n=2}^{\infty} I_n n(n-1),$$

$$d = \sum_{n=3}^{\infty} G_n n(n-1)(n-2), \quad e = \frac{1}{2} \sum_{n=3}^{\infty} H_n n(n-1)(n-2), \quad f = \sum_{n=3}^{\infty} I_n n(n-1)(n-2).$$

The two linear equations Eq. (20) have a non-trivial solution if and only if the following equation is satisfied:

$$\Delta = (a + \kappa b)f - (d + \kappa e)c = 0. \tag{21}$$

Eq. (21) is the characteristic equation for the problem described by Eqs. (9) and (10).

6. Argand diagram

Now that the characteristic equation Eq. (21) has been obtained, its roots λ have to be analysed to draw a conclusion on the riser stability. The most common way to do so is to make use of an Argand diagram [7]. In this diagram, the real and imaginary parts of the natural frequency ω are plotted parametrically, as they depend on one of the system parameters. Normally, the flow velocity V is used as such a parameter. In this paper, along with V, the dimensionless external damping is employed as the parameter to plot a part of the Argand diagram. The natural frequency ω is related to the eigenvalue λ as, $\omega = \mathrm{i}\lambda$. Note that if the imaginary part of a natural frequency ω is smaller than zero, the system is unstable.

At the first step of the analysis, both the fluid velocity and the external damping are disregarded. The system possesses in this case only real natural frequencies, which can be easily found numerically. These natural frequencies equal the resonance frequencies of an undamped cantilever beam with varying tension. As the second step, the damping is gradually increased, keeping the velocity zero, and the accompanying complex values of the natural frequencies are computed and plotted in the Argand diagram. As expected, all complex natural frequencies acquire positive imaginary part, implying that the pipe is stable. Once the damping reaches its 'true' (assumed in the present analysis) value, the fluid velocity is gradually increased from zero. As a result, the imaginary part of the complex natural frequencies decreases with increasing fluid velocity. At a certain velocity, the imaginary part of some natural frequencies becomes negative, implying that the pipe becomes unstable. For constructing the Argand diagram, the system parameters that are shown in Table 1 are used. The internal pressure is taken as independent of the internal fluid velocity, $C^{(1)} = 0$. The Argand diagram is presented schematically in Fig. 2. Only the first four natural frequencies are plotted. The paths of the other natural frequencies have a similar shape as those of the second, third and fourth natural frequencies. The smallest fluid velocity for which the natural frequency has a negative imaginary part is denoted as the critical

Table 1
Parameters used in the calculations

Parameter				Dimensionless parameter	
EI	1.00×10^9 N m^2	L	100 m	α	10.0
m_f	1.00×10^3 kg/m	ρ_f	1.00×10^3 kg/m^3	β	1.83
m_a	1.00×10^3 kg/m	D_0	1.00 m	γ	2.89
m_r	1.00×10^3 kg/m	$\check{C}_d$	1.00 m/s	κ	0.100
T_{top}	1.00×10^6 N	C_{fl}	1.00×10^6 N m/rad		

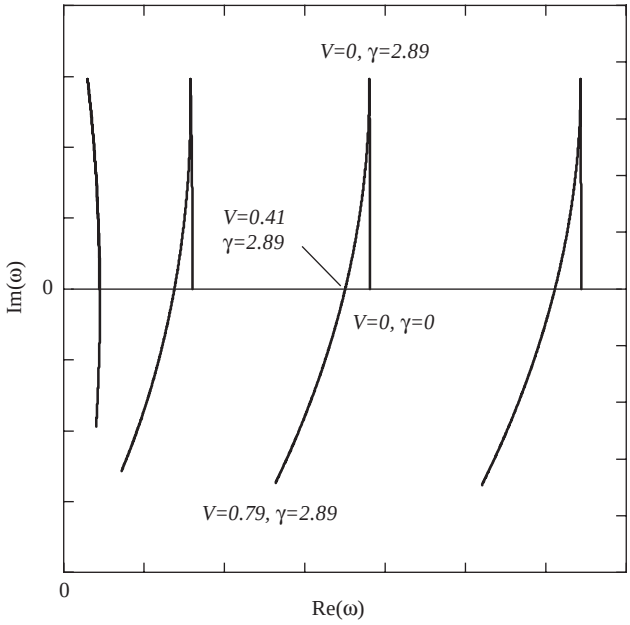

Fig. 2. Argand diagram for the first four natural frequencies.

velocity V^*. The paths of all the natural frequencies, except the first one, intersect the real ω-axis at almost the same fluid velocity. This implies that the corresponding modes become unstable at the same fluid velocity.

Using the Argand diagram, the influence of the description of the internal pressure on the system stability can be analysed. In Fig. 3, the second natural frequency of the system is shown for the three different descriptions of the internal pressure as mentioned before. As can be seen, the real part of the complex natural frequency changes drastically by using different descriptions of the internal pressure. However, the critical velocity V^* is hardly different for these three descriptions (the deviation is less than 2%). Similar observations can be made for all other natural frequencies, and, hence, the influence is marginal of the description of the internal pressure on the system stability. This means that the negative pressurisation cannot be considered as the reason for the stable behaviour of the free-hanging riser, which has been found experimentally. What can be a reason for the observed stable behaviour is the external hydrodynamic drag. This drag can greatly influence the stability of the pipe at hand, since it induces the energy loss all over the length of the pipe, while the energy can be gained at the pipe ends only [1,2].

In the next section, the stabilising effect of this drag is studied by a D-decomposition method, developed by Neimark [9] (see Ref. [10]). The main advantage of this method relative to the Argand diagram is that it does not require searching for complex zeroes of a complex function. The stability can be analysed using the D-decomposition method by just considering the imaginary axis of the complex λ-plane (the plane of complex eigenvalues). This increases the accuracy of the stability analysis and, in some cases, the calculation speed. As shown in the following sections, the D-decomposition method is especially efficient in combination with the Argand diagram.

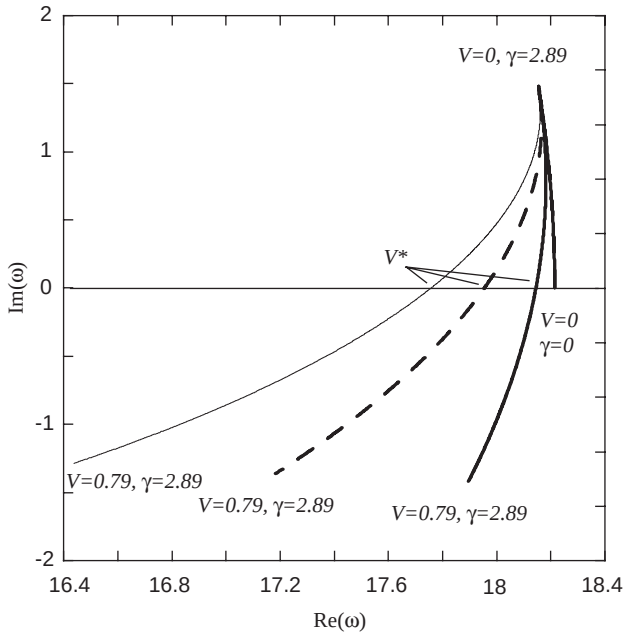

Fig. 3. Argand diagram for the second natural frequency and for three descriptions of the internal pressure ($C^{(1)} = 0$, — $C^{(2)} = V^2$, ▬ $C^{(3)} = V^2/2 - -$).

7. D-decomposition method

The D-decomposition method utilises the fact that the stability of a linear system is fully determined by the sign of the real part of its eigenvalues λ (Eq. (11)). The eigenvalues which correspond to unstable vibrations are located in the right-half plane of the complex λ-plane, see Fig. 4. Consequently, the imaginary axis of this plane, $\lambda = \mathrm{i}\Omega, \Omega \in \Re$ is the boundary that separates the "stable" and "unstable" eigenvalues (roots with $\mathrm{Re}(\lambda) < 0$ and $\mathrm{Re}(\lambda) > 0$, respectively). Assume now that the characteristic equation contains a parameter P that can be expressed explicitly. Such expression can be then used as a mapping rule to map the imaginary axis of the λ-plane onto the complex plane of the parameter P, as sketched in Fig. 4. The frequency Ω serves as the parameter of this mapping. The resulting mapped lines, which are referred to as D-decomposition lines, break the P-plane into domains with different number of "unstable" eigenvalues. Within a domain, this number may not vary.

Shading the right side of the imaginary axis of the λ-plane (the side of "unstable" eigenvalues), and keeping the shading at the corresponding side of the D-decomposition lines, the information contained in the decomposed P-plane can be enriched. With this shading, it becomes known that passing through a D-decomposition line in the direction of shading corresponds to the gain of one additional "unstable" eigenvalue by the characteristic equation. Thus, if the number of the "unstable" eigenvalues is known for only one (arbitrary) value of the parameter P, the D-decomposed P-plane allows to draw a conclusion on the stability of the system for all admissible values of this parameter at once.

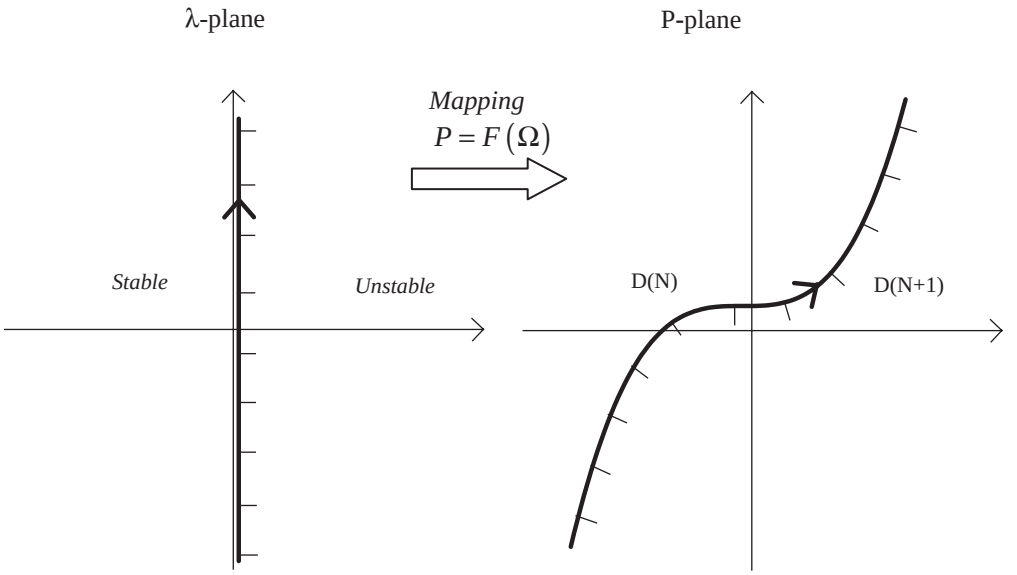

Fig. 4. Graphical representation of the D-decomposition method. The notation $D(N)$ implies that there are N "unstable" eigenvalues in the domain.

For the free-hanging riser conveying fluid, the dimensionless rotational spring stiffness κ can serve as the parameter P, since it can be readily expressed from the characteristic equation (21) to give

$$\kappa = \frac{-af + cd}{-ce + bf}. \tag{22}$$

The D-decomposition of the κ-plane is depicted in Figs. 5 and 6 for two velocities of the fluid, namely $V = 0.32$ and 0.95, respectively. The system parameters used in calculations are shown in Table 1. The internal pressure is taken as independent of the internal fluid velocity, $C^{(1)} = 0$ (the other two descriptions give almost the same result). Note that in both figures only the positive part of the real axis has physical meaning, since κ is the stiffness of the rotational spring. Only the key (low-frequency) part of the D-decomposition curves is plotted in the figures. Taking higher frequencies into account would lead to a larger number of quasi-circles both in the lower and upper half planes. These circles do not change the result of the stability analysis.

Although the D-composition curves in Figs. 5 and 6 have qualitatively the same shapes, these curves run with the increase of Ω in opposite directions. In both figures, the D-decomposition curves do not cross the positive part of the real axis. So, in one run with the D-decomposition method, it is easily concluded that the riser stability does not depend on the stiffness of the rotational spring. It would be much more laborious to draw the same conclusion by using only the Argand diagram. The question remains if the pipe is stable or unstable for all real and positive values of the rotational spring. To answer this question, it is sufficient to determine the number N of unstable roots for one particular stiffness of the rotational spring. For the problem at hand, this can be conveniently done by making use of the Argand diagram (note that studying other stability

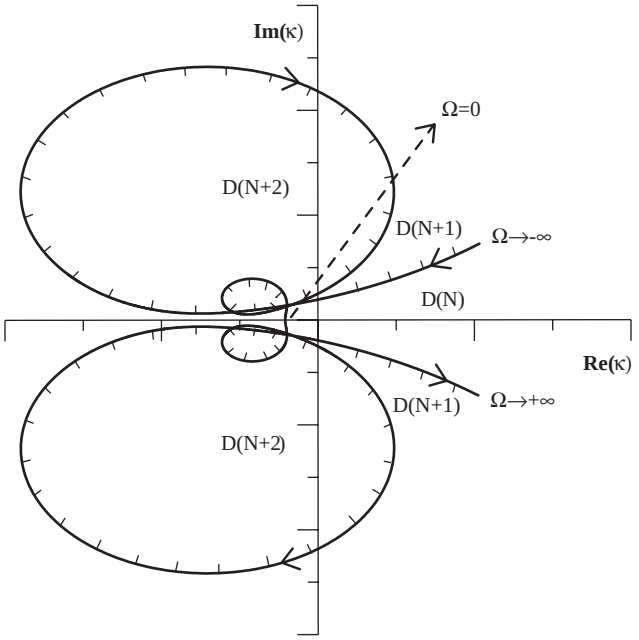

Fig. 5. D-decomposition of the κ-plane for $V = 0.32$.

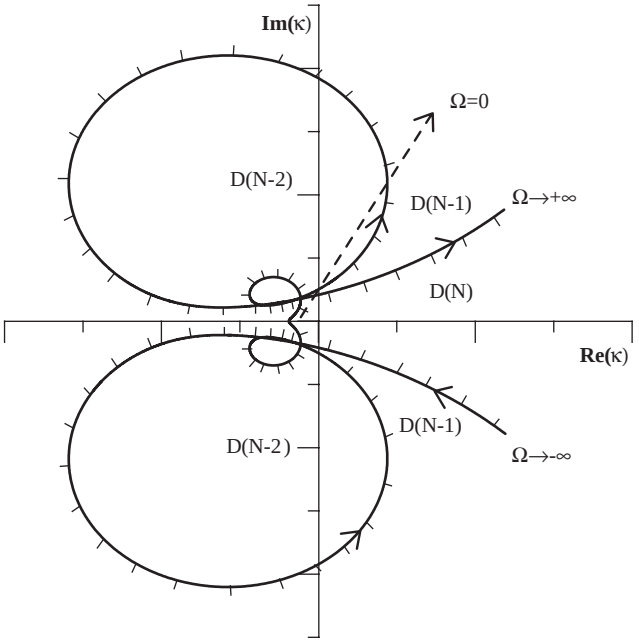

Fig. 6. D-decomposition of the κ-plane for $V = 0.95$.

problems, the number of unstable roots for a particular set of parameters can be found using physical considerations [14] or the principle of the argument [12]).

As follows from Fig. 2, the pipe is stable if the flow velocity belongs to the interval $0 \leqslant V < V^*$, and is unstable if $V > V^*$, where V^* is the critical velocity. For the parameters given in Table 1, this critical velocity is $V^* \approx 0.41$, which is greater than $V = 0.32$ (Fig. 5) and smaller than $V = 0.95$ (Fig. 6). Thus, combining the information containing in Figs. 2 and 5, it can be concluded that the pipe is *stable* independently of the flexjoint stiffness if V=0.32. On the contrary, as follows from Figs. 2 and 6, the pipe is unstable if $V = 0.95$, again independently of the flexjoint stiffness. These conclusions can be generalised by performing the D-decomposition of the κ-plane for other velocities V of the flow through the pipe. This decomposition shows that, independently of the flexjoint stiffness, the pipe is stable if $0 \leqslant V < V^*$ and is unstable if $V > V^*$.

Thus, applying the D-decomposition method, the critical velocity V^* can be easily found, which separates the stable and unstable behaviours of the riser. To this end, it is sufficient to track the half-plane (upper or lower) to which the D-decomposition curve runs as the frequency Ω is increased from zero. If the curve runs to the lower half-plane, then the pipe is stable. The flow velocity, at which the curve starts to run to the upper half-plane is the critical velocity V^*. This approach is used in the next section to investigate the effect of fluid pressurisation at the inlet and of the hydrodynamic drag (external damping) on the pipe stability.

8. Effect of fluid pressurisation and external damping

As shown in the previous sections, both the Argand diagram and the D-decomposition method can be used to compute the critical velocity after which the system becomes unstable. Here we use the D-decomposition method to analyse the critical velocity. This velocity depends on all parameters of the system, including the difference between the external and internal hydrostatic pressure and the amount of external damping γ. The dependence of the critical velocity on the external damping breaks the plane (V, γ) as shown in Fig. 7. In this figure, the critical velocity is presented for three values of the pressure difference, which are studied in this paper. This dependence is obtained using parameters given in Table 1.

From Fig. 7 the conclusion should be drawn that the effect of the internal fluid pressure is small, especially, for low fluid velocities. This means that the negative pressurisation cannot be considered as the reason for the stable behaviour of the free-hanging riser, which has been found experimentally. From Fig. 7 it is also clear that the external damping has a much more significant influence on the system stability. Without external damping ($\gamma = 0$), the system is unstable for all fluid velocities, irrespective of the description of the internal pressure. On the contrary, with the external damping, a stable range of velocities is found, for which the system behaves stable, as was observed in the experiments.

As mentioned in the introduction, the hydrodynamic drag caused by the surrounding water is described in this paper by a simplistic linearised expression, which does not allow to draw any quantitative conclusions. In order to prove that this damping (drag) is indeed the cause of the discrepancy between theory and experiment, experiments should be carried out to check if fluid velocities which should lead to instability, in accordance with the results in Fig. 7, agree with

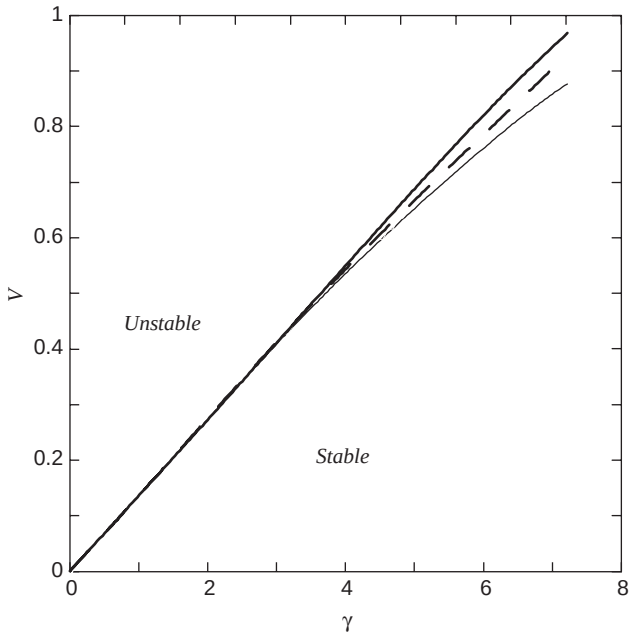

Fig. 7. The dimensionless critical velocity for three descriptions of the internal pressure as a function of the external damping γ ($C^{(1)} = 0$, — $C^{(2)} = V^2$, ▬ $C^{(3)} = V^2/2$ – –).

measurements. If not, the model for the riser should be improved by taking into account a nonlinear description of the drag, including the drag dependence on the Reynolds number.

9. Conclusions

In this paper, the stability of a free-hanging riser conveying fluid has been considered. It has been proven that the existing contradiction between theory (predicts instability for small fluid velocities) and experiments (show stable behaviour for small fluid velocities) cannot be explained by the negative pressurisation at the riser inlet. The stability analysis that has been carried out in this paper has shown a marginal effect of this depressurisation.

The difference between theory and experiment might be explained by the energy dissipation caused by the hydrodynamic drag, which the riser experiences while moving in water. It would be advisable to carry out experiments to check if the critical fluid velocities agree with the results of this paper (see Fig. 7). If not, the model for the riser should be improved by taking into account a more realistic, nonlinear description of the drag, which has been linearised in this paper.

Acknowledgements

This research is supported by the Technology Foundation STW, Applied Science Division of NWO and the technology programme of the Ministry of Economic Affairs. The authors thank Professor J.A. Battjes for his helpful suggestions.

References

[1] S.-Y. Lee, C.D. Mote, A generalized treatment of the energetics of translating continua—part I: strings and tensioned pipes, *Journal of Sound and Vibration* 204 (1997) 717–734.
[2] S.-Y. Lee, C.D. Mote, A generalized treatment of the energetics of translating continua—part II: beams and fluid conveying pipes, *Journal of Sound and Vibration* 204 (1997) 735–753.
[3] J.S. Chung, A.K. Whitney, W.A. Loden, Nonlinear transient motion of deep ocean mining pipe, *Journal of Energy Resources Technology* 103 (1981) 2–10.
[4] M.P. Païdoussis, T.P. Luu, Dynamics of a pipe aspirating fluid, such as might be used in ocean mining, *Journal of Energy Resources Technology* 107 (1985) 250–255.
[5] J.H. Sällström, B.Å. Åkesson, Fluid-conveying damped Rayleigh–Timoshenko beams in transverse vibration analyzed by use of an exact finite element—part I: theory, *Journal of Fluids and Structures* 4 (1990) 561–572.
[6] M. Kangaspuoskari, J. Laukkanen, A. Pramila, The effect of feedback control on critical velocity of cantilevered pipes aspirating fluid, *Journal of Fluids and Structures* 7 (1993) 707–715.
[7] M.P. Païdoussis, *Fluid–Structure Interactions*: *Slender Structures and Axial Flow*, vol. 1, Academic Press, London, 1998.
[8] M.P. Païdoussis, Aspirating pipes do not flutter at infinitesimally small flow, *Journal of Fluids and Structures* 13 (1999) 419–425.
[9] Y.I. Neimark, *Dynamic Systems and Controllable Processes*, Nauka, Moscow, 1978 (in Russian).
[10] Y.I. Neimark, V.I. Golumov, M.M. Kogan, *Mathematical Models in Natural Science and Engineering*, Springer, Berlin, 2003.
[11] A.V. Metrikine, K. Popp, Instability of vibrations of an oscillator moving along a beam on an elastic half-space, *European Journal of Mechanics A/Solids* (1999) 331–349.
[12] S.N. Verichev, A.V. Metrikine, Instability of a moving bogie on a flexibly supported Timoshenko beam, *Journal of Sound and Vibration* 253 (2002) 653–668.
[13] T. Huang, D.W. Dareing, Natural frequencies of marine drilling risers, *Journal of Petroleum Technology* (1976) 813–818.
[14] A.V. Metrikine, H.A. Dieterman, Instability of vibrations of a mass moving uniformly along an axially compressed beam on a visco-elastic foundation, *Journal of Sound and Vibration* 201 (1997) 567–576.